JOURNAL OF GUIDANCE, CONTROL, AND DYNAMICS
Vol. 29, No. 6, November–December 2006

Optimal Balanced-Energy Formation Flying Maneuvers

Amirreza Rahmani* and Mehran Mesbahi†
University of Washington, Seattle, Washington 98195-2400
and
Fred Y. Hadaegh‡
Jet Propulsion Laboratory, California Institute of Technology, Pasadena, California 91109-8099

DOI: 10.2514/1.19199

Spacecraft formation flying has recently been proposed and examined in the space systems community as a promising alternative to monolithic and often large space structures. Optimal balanced-energy control of such distributed space systems potentially increases their lifetime and can serve as an important baseline in mission feasibility studies. In this paper, an optimal balanced-energy control strategy for two- and three- spacecraft distributed space systems is proposed. Along the way, we will delineate relevant mission scenarios in deep space, as well as those that operate in Earth's gravitational sphere of influence. Simulation results demonstrating the ramifications of our theoretical analysis are also provided.

I. Introduction

FORMATION flying has been identified as a key technology for many of the future space missions by National Aeronautics and Space Administration, European Space Agency, and several military and civilian space sectors [1,2] (see also [3–10]). It is envisioned that to improve reliability and science return, many near-Earth and deep-space missions can be architected as multiple, less expensive, cooperative spacecraft flying in formation. Spacecraft formation flying, on the other hand, involves maintaining a precise relative geometry among the spacecraft units over an extended period of time using the onboard limited resources. In fact, the multiple spacecraft control system should have the ability to accomplish two basic tasks: formation maneuver planning and formation keeping. In both cases, optimized, and in many scenarios, balanced-energy consumption is among the most crucial control objectives. This is due to the fact that the lifetime of a formation flying mission not only depends on the individual spacecraft energy consumption but also on the energy consumed on each spacecraft with respect to others. In some missions, the balanced-energy consideration becomes even more critical: if one of the spacecraft runs out of fuel faster, the entire distributed system becomes nonoperational. For example, in a popular strategy for formation flying based on a leader-following control architecture [11,12], the formation lifetime is dictated by the fuel usage of the follower spacecraft. A possible remedy for this problem is to switch the leader assignment when the total control effort exerted by one spacecraft significantly exceeds that of the others. This switching can be accomplished autonomously by the formation manager or via the ground station. In the former case, the formation manager tracks the vehicle resources and periodically adjusts the control parameters to satisfy multiple mission objectives, including balancing the fuel usage [13]. In [14], it was observed that defining a virtual center for the formation and tracking the weighted average motion of the system, alleviates the fuel usage imbalance between the leader and the follower spacecraft. In [15], Vadali et al. introduced modified reference trajectories for the Hill's dynamics to ensure balanced fuel consumption for the satellites while maintaining the desired orbits.

In the present paper, we address the optimized balanced-energy maneuvers for a group of two- and three-spacecraft formations, commanded to reconfigure to new relative positions via optimal control techniques. Formation planning and formation keeping maneuvers for deep-space and near-Earth orbit scenarios are then investigated. We conclude the paper by providing a set of numerical simulations to delineate our theoretical analysis.

II. Motivation

In this section, we provide a motivational example for the balanced-energy dual-spacecraft formation flying in the setting of space-borne optical interferometry. Space-borne optical interferometry holds the promise of revolutionizing our understanding of the origins and evolution of planetary systems. It has been argued that by enabling direct imaging of distant stars and their orbiting planets, optical interferometry provides a unique opportunity into characterizing the size, temperature, and the orbital parameters of heavenly bodies, possibly identifying their habitable zones [1].

To see the relevance of multiple spacecraft formation flying to imaging distant celestial bodies, recall that imaging refers to the evaluation of the intensity profile for a source object. On the other hand, through the well-known van Cittert–Zernike formula [16,17], the source intensity is related to the inverse Fourier transform of the mutual coherence function μ by

$$\underbrace{\mathcal{I}(X,Y)}_{\text{intensity}} = \int_u \int_v \underbrace{\mu(u,v)}_{\text{mutual coherence}} e^{i2\pi(uX+vY)} dv du \tag{1}$$

rather conveniently, the mutual coherence is measurable through specialized optical instruments [18]. We note that in Eq. (1), one has

$$u = \frac{1}{z\lambda}(x_1 - x_2) \quad \text{and} \quad v = \frac{1}{z\lambda}(y_1 - y_2) \tag{2}$$

where λ and z are, respectively, the wavelength of the light emitted by the source (star) and the corresponding measurement distance; (x_1, y_1), (x_2, y_2) are the positions of the aperture in the physical space. Imaging a light source thus amounts to the evaluation of the mutual coherence function μ over a disk of infinite radius in the uv-plane [referring to the arguments of the integral in Eq. (1)]. Approximating the intensity profile for the light source can now be accomplished by choosing a disk of *finite* radius and evaluating the

Received 28 July 2005; revision received 24 February 2006; accepted for publication 25 February 2006.

*Graduate Student, Department of Aeronautics and Astronautics, P.O. Box 352400. Student Member AIAA; arahmani@aa.washington.edu.

†Associate Professor, Department of Aeronautics and Astronautics, P.O. Box 352400. Member AIAA; mesbahi @aa.washington.edu.

‡Senior Research Scientist and Group Supervisor, Mail Stop 198-326, 4800 Oak Grove Drive. Fellow AIAA; fred.y.hadaegh@jpl.nasa.gov

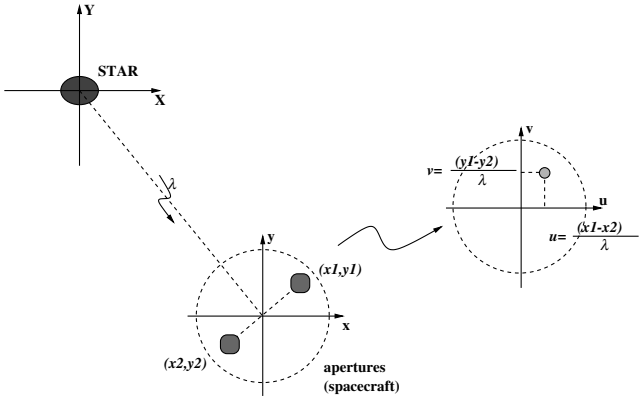

Fig. 1 Imaging a star via optical interferometry ($z = 1$).

mutual coherence function at a finite number of uv-points. The selection of the uv-points for each light source, based on some a priori knowledge about the source, is of independent interest and has been considered for example in [19]. For the purpose of our discussion, we assume that for each source, the set of uv-points has already been specified. Hence, for N stars, we have been supplied with the list

$$\underbrace{(u_1, v_1), \ldots, (u_{n_1}, v_{n_1})}_{\text{star1}}, \ \ldots, \underbrace{(u_1, v_1), \ldots, (u_{n_N}, v_{n_N})}_{\text{star } N}$$

where n_j is the number of uv-points for star j. Consider now the scenario where each aperture is placed on a separate spacecraft (Fig. 1). The process of moving the dual-spacecraft (aperture) in a formation to sample the specified set of points in the uv-plane is called uv-plane coverage [19].

In the meantime, the geometry of the optical interferometry mission is dictated by the path lengths that the starlight travels to the location where the image is finally synthesized. For example, NASA's formerly proposed Starlight Mission consisted of two spacecraft in an Earth-trailing orbit around the sun [3]; one spacecraft is placed at the focus of a paraboloid and the other moves on its perimeter (Fig. 2). The spacecraft at a paraboloid's focus, the combiner, carries the instruments necessary for collecting and interfering light rays. The other spacecraft, the collector, carries the instruments for collecting light rays and redirecting them to the combiner spacecraft. We note that based on the number of spacecraft in the formation and the mission science objectives, other geometrical configurations can be adopted for optical interferometry missions. For example, for planet finding, and ultimately, for planet imaging, a nulling capability is also required, necessitating a formation of five spacecraft [1].

Having identified the set of uv-points for an imaging mission, the next step is to map these points, based on the geometry of the mission, to the desired inertial positions of the dual-spacecraft. Hence, the set of u, v-points for imaging a given star translates to a sequence of relative distance vectors z in the Euclidean space (see [20] for more details on the required transformations). In other words, the uv-plane coverage for N stars reduces to a set of relative distance vectors of the form

$$\underbrace{z_1, \ldots, z_{n_1}}_{\text{star1}}, \ldots, \underbrace{z_1, \ldots, z_{n_2}}_{\text{star2}}, \ldots, \underbrace{z_1 z_1, \ldots, z_{n_N}}_{\text{star } N}$$

where n_j is the number of specified uv-points for star j. Approximating the intensity profile for a light source leads to a consecutive set of formation reconfigurations that map to the desired set of uv-points.

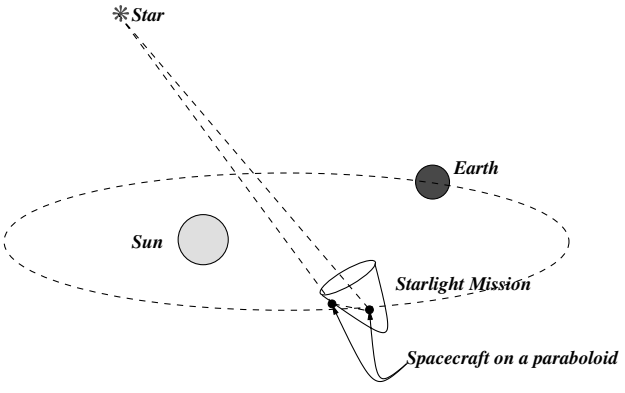

Fig. 2 Starlight in a heliocentric orbit.

III. Dual-Spacecraft Balanced-Fuel Maneuvers

Consider a two-spacecraft formation with its translational motion abstracted by the double integrator dynamics

$$\dot{x}_i(t) = Ax_i(t) + B_i u_i(t), \qquad i = 1, 2 \tag{3}$$

where each $x_i \in \mathbb{R}^6$ consists of position and velocity components, $A \in \mathbb{R}^{6\times 6}$, and $B_i = (1/m_i)[0\ I]^T \in \mathbb{R}^{6\times 3}$. In Sec. III.B, we will address the range of validity for the double integrator dynamics with respect to the formation inertial position and its reconfiguration maneuver time.

For two-spacecraft formations, let us define the relative state as the vector difference $z(t) = x_1(t) - x_2(t)$. Thus,

$$\dot{z}(t) = Az(t) + Bu(t) \tag{4}$$

where $B = [B_1 - B_2]$ and $u(t) = [u_1(t) u_2(t)]^T$. As discussed in Sec. I, our objective in this paper will be to minimize the overall energy consumption in a "balanced" manner. This goal can be expressed via an objective functional of the form

$$\begin{aligned}\mathcal{J}(u) &= \int_{t_0}^{t_f} \{u_1(t)^T R_1 u_1(t) + u_2(t)^T R_2 u_2(t) + [u_2(t) \\ &\quad - u_1(t)]^T \hat{R}[u_2(t) - u_1(t)]\}\, \mathrm{d}t \\ &= \int_{t_0}^{t_f} u^T(t) \begin{bmatrix} R_1 + \hat{R} & -\hat{R} \\ -\hat{R} & R_2 + \hat{R} \end{bmatrix} u(t)\, \mathrm{d}t \\ &= \int_{t_0}^{t_f} u(t)^T R u(t)\, \mathrm{d}t \end{aligned} \tag{5}$$

where R_1, R_2, and $\hat{R}$ are weighting matrices of appropriate dimensions. The relation between these weighting matrices provides a design decision, reflecting the relative importance of minimizing the individual spacecraft energy consumption and balancing this consumption among the different spacecraft. Having selected these weights, the balanced-energy spacecraft reconfiguration problem is now defined as

$$\min_u \mathcal{J}(u)$$

subject to the dynamic constraint (4) and the boundary conditions $z(t_0) = z_0$ and $z(t_f) = z_f$.

A. Optimal Control Strategy

To solve the balanced-energy reconfiguration problem for a dual-spacecraft system, we first consider the Hamiltonian

$$\mathcal{H}(z, u, \lambda) = u^T R u + \lambda^T (Az + Bu) \tag{6}$$

For optimality conditions, we then have

$$\dot{\lambda}(t) = -\frac{\partial \mathcal{H}}{\partial z} = -A^T \lambda(t) \tag{7}$$

$$\dot{z}(t) = \frac{\partial \mathcal{H}}{\partial \lambda} = Az(t) + Bu(t) \tag{8}$$

$$0 = \frac{\partial \mathcal{H}}{\partial \boldsymbol{u}} = 2R\boldsymbol{u}(t) + B^T\lambda(t) \tag{9}$$

Hence,

$$\lambda(t) = e^{-A^T t}\boldsymbol{y} = (I - tA^T)\boldsymbol{y}$$

where $\boldsymbol{y}$ is a constant vector of proper dimension, determined by the boundary conditions of the costate λ. Solving Eq. (9) for the control u and substituting it back in Eq. (8) leads to

$$\dot{z}(t) = Az(t) - \frac{1}{2}BR^{-1}B^T(I - tA^T)\boldsymbol{y}(t) \tag{10}$$

In the meantime, as R is a block partitioned matrix, its inverse can be computed by

$$R^{-1} = \begin{bmatrix} R_{11} & R_{12} \\ R_{21} & R_{22} \end{bmatrix}^{-1} = \begin{bmatrix} \bar{R}_{11} & \bar{R}_{12} \\ \bar{R}_{21} & \bar{R}_{22} \end{bmatrix}$$

with

$$\begin{aligned}
\bar{R}_{11} &= (R_{11} - R_{12}R_{22}^{-1}R_{21})^{-1}, \\
\bar{R}_{12} &= R_{11}^{-1}R_{12}(R_{21}R_{11}^{-1}R_{12} - R_{22})^{-1}, \\
\bar{R}_{21} &= (R_{21}R_{11}^{-1}R_{12} - R_{22})^{-1}R_{21}R_{11}^{-1}, \\
\bar{R}_{22} &= (R_{22} - R_{21}|R_{11}^{-1}R_{12})^{-1}
\end{aligned}$$

Now by solving the differential Eq. (10) for $z(t)$ we obtain

$$z(t) = e^{A(t-t_0)}z(t_0) - \frac{1}{2}\int_0^{t-t_0} e^{A\tau}BR^{-1}B^T[I - (t-\tau)A^T]\boldsymbol{y}(\tau)\,\mathrm{d}\tau$$

Because of the special structure of the matrix A we know that

$$e^{A(t-t_0)} = I + (t - t_0)A$$

since $A^n = 0$ for all positive integers $n > 1$ and hence

$$\begin{aligned}
z(t) &= [I + (t-t_0)A]z(t_0) \\
&\quad + \frac{1}{2}\int_0^{t-t_0} -(I + \tau A)BR^{-1}B^T[I - (t-\tau)A^T]\boldsymbol{y}(\tau)\,\mathrm{d}\tau
\end{aligned}$$

Concurrently,

$$BR^{-1}B^T = \begin{pmatrix} 0 & 0 \\ 0 & \bar{R} \end{pmatrix} \tag{11}$$

and

$$I + (t - t_0)A = \begin{pmatrix} I & (t-t_0)I \\ 0 & I \end{pmatrix}$$

thereby,

$$\begin{aligned}
z(t) &= \begin{bmatrix} I & (t-t_0)I \\ 0 & I \end{bmatrix} z(t_0) \\
&\quad + \frac{1}{2}\begin{bmatrix} \frac{1}{6}(t-t_0)^2(t+2t_0)\bar{R} & -\frac{1}{2}(t-t_0)^2\bar{R} \\ \frac{1}{2}(t-t_0)(t+t_0)\bar{R} & -(t-t_0)\bar{R} \end{bmatrix}\boldsymbol{y}
\end{aligned} \tag{12}$$

where

$$\bar{R} = \frac{1}{m_1^2}\bar{R}_{11} - \frac{1}{m_1 m_2}\bar{R}_{12} - \frac{1}{m_1 m_2}\bar{R}_{21} + \frac{1}{m_2^2}\bar{R}_{22}$$

Consider the case where $R_1 = R_2 = I$ and $\hat{R} = \beta I$ in Eq. (5). Then

$$\bar{R} = \frac{1}{2\beta + 1}\left(\frac{1+\beta}{m_1^2} - 2\frac{\beta}{m_1 m_2} + \frac{1+\beta}{m_2^2}\right)I \tag{13}$$

and $z(t)$ assumes the form

$$z(t) = \begin{bmatrix} I & (t-t_0)I \\ 0 & I \end{bmatrix} z(t_0) + \frac{1}{2(2\beta+1)}M(t)\boldsymbol{y} \tag{14}$$

with

$$\begin{aligned}
M(t) &= \left(\frac{1+\beta}{m_1^2} - \frac{2\beta}{m_1 m_2} + \frac{1+\beta}{m_2^2}\right) \\
&\quad \times \begin{bmatrix} \frac{1}{6}(t-t_0)^2(t+2t_0)I & -\frac{1}{2}(t-t_0)^2 I \\ \frac{1}{2}(t-t_0)(t+t_0)I & -(t-t_0)I \end{bmatrix}
\end{aligned} \tag{15}$$

Having specified the initial and final conditions $z(t_0)$ and $z(t_f)$, one can then solve for the constant vector $\boldsymbol{y}$ as

$$\boldsymbol{y} = 2(2\beta+1)M(t_f)^{-1}\left(z(t_f) - \begin{bmatrix} I & (t_f - t_0)I \\ 0 & I \end{bmatrix} z(t_0)\right)$$

However, from Eq. (9) one has

$$\boldsymbol{u}(t) = -\frac{1}{2}R^{-1}B^T(I - tA^T)\boldsymbol{y} \tag{16}$$

and thus the optimal controls can explicitly be expressed as

$$\begin{aligned}
\boldsymbol{u}(t) &= -\frac{m_1^2 m_2^2}{(m_1^2 + m_2^2)(1+\beta) - 2\beta m_1 m_2} \\
&\quad \times \begin{bmatrix} -t\left(\frac{1+\beta}{m_1} - \frac{\beta}{m_2}\right)I & \left(\frac{1+\beta}{m_1} - \frac{\beta}{m_2}\right)I \\ t\left(\frac{1+\beta}{m_2} - \frac{\beta}{m_1}\right)I & -\left(\frac{1+\beta}{m_2} - \frac{\beta}{m_1}\right)I \end{bmatrix} \\
&\quad \times \begin{bmatrix} -\frac{12}{t_f{}^3}I & \frac{6}{t_f{}^2}I \\ -\frac{6}{t_f{}^2}I & \frac{2}{t_f}I \end{bmatrix}\left(z(t_f) - \begin{bmatrix} I & t_f I \\ 0 & I \end{bmatrix} z(t_0)\right)
\end{aligned} \tag{17}$$

In the case where $m_1 = m_2$, Eq. (17) reduces to

$$\begin{aligned}
\boldsymbol{u}(t) &= -\frac{m_1}{2}\begin{bmatrix} -tI & I \\ tI & -I \end{bmatrix} \\
&\quad \times \begin{bmatrix} -\frac{12}{t_f{}^3}I & \frac{6}{t_f{}^2}I \\ -\frac{6}{t_f{}^2}I & \frac{2}{t_f}I \end{bmatrix}\left(z(t_f) - \begin{bmatrix} I & t_f I \\ 0 & I \end{bmatrix} z(t_0)\right)
\end{aligned} \tag{18}$$

implying the intuitive result that the dual-spacecraft controls are equal in magnitude but point in opposite directions during the reconfiguration maneuver.

It is instructive to note that the optimal balanced-energy control critically depends on the relation between the weighting matrices R_1, R_2, and $\hat{R}$ in Eq. (5). For example, in the case where $R_1 = R_2 = I$ and $\hat{R} = \beta I$, the parameter β captures the relative importance of balancing the spacecraft energy consumption to minimizing its total usage. Figure 3 depicts the fuel consumption for the reconfiguration of a pair of spacecraft, with mass values of 200 and 100 kg, respectively, for a maneuver time of 1200 s.[§] The specific impulse (Isp) for each spacecraft is chosen to be 400 s. In this figure, the solid curve depicts the percentage of the total fuel consumption to that consumed when the parameter β is arbitrarily large in Eq. (17). The dashed curve depicts the percentage of the difference between the individual spacecraft fuel consumption to the total fuel usage.

The trade-off between optimality of the individual spacecraft fuel consumption and balancing the fuel usage among them can be formalized as follows. Let

[§]Although our analysis is based on the spacecraft energy consumption, for practical relevance, our comparative simulations are done with respect to the spacecraft fuel usage.

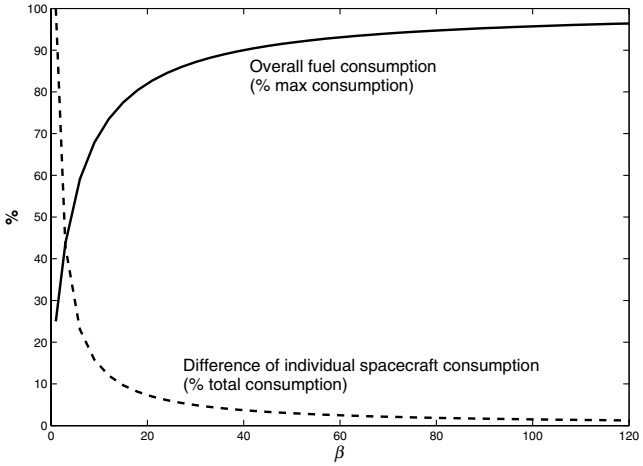

Fig. 3 Balancing and minimizing the total fuel consumption for the reconfiguration of a pair of spacecraft.

$$\mathcal{J}_0(\boldsymbol{u}) := \int_{t_0}^{t_f} \boldsymbol{u}(t)^T \begin{bmatrix} R_1 & 0 \\ 0 & R_2 \end{bmatrix} \boldsymbol{u}(t)\,\mathrm{d}t \quad \text{and}$$

$$\mathcal{J}_b(\boldsymbol{u}) := \int_{t_0}^{t_f} \boldsymbol{u}(t)^T \begin{bmatrix} \hat{R} & -\hat{R} \\ -\hat{R} & \hat{R} \end{bmatrix} \boldsymbol{u}(t)\,\mathrm{d}t$$

Thus, for all u, $\mathcal{J}(\boldsymbol{u}) = \mathcal{J}_0(\boldsymbol{u}) + \mathcal{J}_b(\boldsymbol{u})$ in Eq. (5). Now, let $\boldsymbol{u}_0^*$ and $\boldsymbol{u}^*$ be the optimal controls that, respectively, minimize $\mathcal{J}_0$ and $\mathcal{J}$, subject to the underlying dynamics and boundary conditions; thereby $\mathcal{J}_0(\boldsymbol{u}_0^*) \le J_0(\boldsymbol{u}^*)$ and $\mathcal{J}(\boldsymbol{u}^*) \le J(\boldsymbol{u}_0^*)$. In particular, $\mathcal{J}_0(\boldsymbol{u}^*) + J_b(\boldsymbol{u}^*) \le \mathcal{J}_0(\boldsymbol{u}_0^*) + \mathcal{J}_b(\boldsymbol{u}_0^*)$ and hence

$$\mathcal{J}_0(\boldsymbol{u}_0^*) \le \mathcal{J}_0(\boldsymbol{u}^*) \le \mathcal{J}_0(\boldsymbol{u}_0^*) + [\mathcal{J}_b(\boldsymbol{u}_0^*) - \mathcal{J}_b(\boldsymbol{u}^*)] \tag{19}$$

Similarly, one has

$$\mathcal{J}(\boldsymbol{u}^*) \le \mathcal{J}(\boldsymbol{u}_0^*) \le \mathcal{J}(\boldsymbol{u}^*) + [\mathcal{J}_b(\boldsymbol{u}_0^*) - \mathcal{J}_b(\boldsymbol{u}^*)] \tag{20}$$

For the case when a spacecraft pair have equal mass values, the difference $\mathcal{J}_b(\boldsymbol{u}_0^*) - \mathcal{J}_b(\boldsymbol{u}^*)$ in the inequality (19) vanishes and the balanced-energy optimal controls coincides with an individually optimal energy solution. This observation can also be deduced from Eq. (18), when the optimal balanced-energy controls becomes independent of the parameter β when $m_1 = m_2$.

We note that the proposed algorithm balances energy consumption for each reconfiguration maneuver. In certain mission scenarios, it might be judicious to balance the energy consumed by the spacecraft units *after* a sequence of prespecified reconfigurations. This problem setup has been considered in [21] where it leads to a traveling salesman-type problem [22].

B. Balanced-Fuel Formation Reconfiguration in Earth's Gravity Well

In the preceding section, we assumed that formation maneuvers occurred in deep space and relied on the double integrator model to capture the formation dynamics. We further delineate the domain of validity of this modeling assumption in this section.

We recall that for circular reference orbits the motion of a dual-spacecraft formation is characterized by the well-known Clohessy–Wiltshire or the Hill's equations [23,24]. In this case, the matrix A in Eq. (3) assumes the form

$$A = \begin{bmatrix} 0 & 0 & 0 & 1 & 0 & 0 \\ 0 & 0 & 0 & 0 & 1 & 0 \\ 0 & 0 & 0 & 0 & 0 & 1 \\ 3n^2 & 0 & 0 & 0 & 2n & 0 \\ n0 & 0 & 0 & -2n & 0 & 0 \\ 0 & 0 & -n^2 & 0 & 0 & 0 \end{bmatrix} \tag{21}$$

where the orbit's natural frequency $n = \sqrt{GM/r^3}$ is specified by the radius of the reference circular orbit r, Earth's mass M, and the universal gravitational constant G. Defining the relative state between the two spacecraft as $\boldsymbol{z}(t) := x_1(t) - x_2(t)$, we are then led to the optimality conditions as in Eqs. (7) and (9). Subsequently, solving Eqs. (7) and (9) for the control term $\boldsymbol{u}$ and substituting it back in Eq. (8), we obtain

$$\dot{\boldsymbol{z}}(t) = A\boldsymbol{z}(t) - \frac{1}{2} B R^{-1} B^T e^{-A^T t} \boldsymbol{y} \tag{22}$$

Using the Jordan transformation, the matrix exponential e^{At} can conveniently be represented as

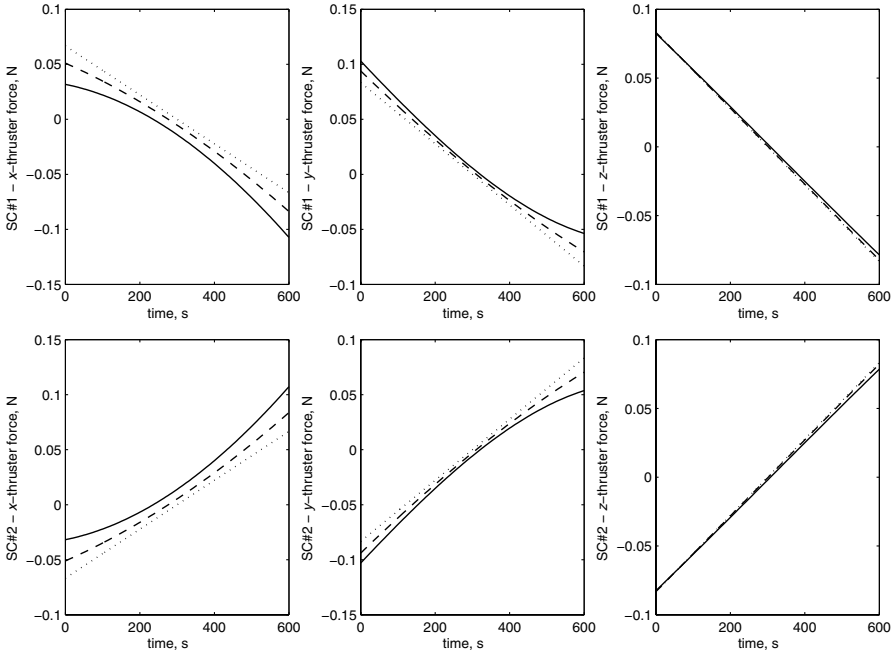

Fig. 4 Case 1: control forces for a dual-spacecraft with identical mass values.

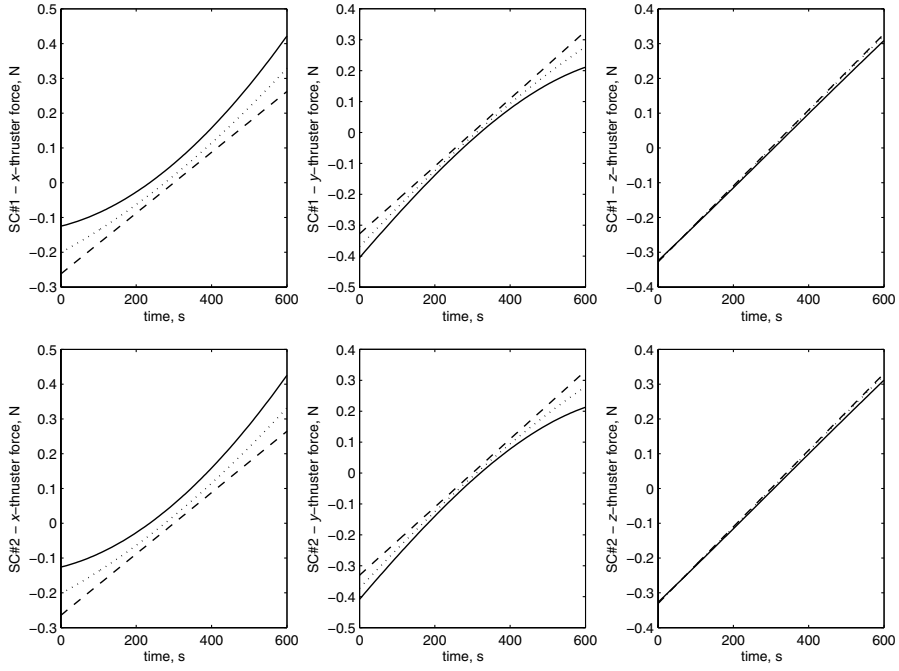

Fig. 5 Case 2: control forces for a dual-spacecraft with distinct mass values.

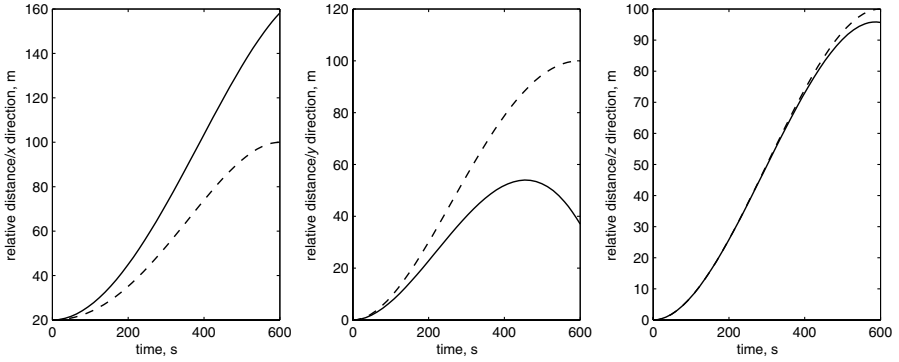

Fig. 6 The relative distance time history for the dual-spacecraft in Case 2.

$$\begin{bmatrix} 4-3\mathcal{C} & 0 & 0 & \frac{\mathcal{S}}{n} & \frac{-2\mathcal{C}+2}{n} & 0 \\ 6\mathcal{S}-6nt & 1 & 0 & \frac{2\mathcal{C}-2}{n} & \frac{-3nt+4\mathcal{S}}{n} & 0 \\ 0 & 0 & \mathcal{C} & 0 & 0 & \frac{\mathcal{S}}{n} \\ 3n\mathcal{S} & 0 & 0 & \mathcal{C} & 2\mathcal{S} & 0 \\ 6n\mathcal{C}-6n & 0 & 0 & -2\mathcal{S} & -3+4\mathcal{C} & 0 \\ 0 & 0 & -n\mathcal{S} & 0 & 0 & \mathcal{C} \end{bmatrix}$$

where $\mathcal{C}=\cos(nt)$ and $\mathcal{S}=\sin(nt)$. In the meantime, solving Eq. (22) leads to

$$\boldsymbol{z}(t)=e^{A(t-t_0)}\boldsymbol{z}(t_0)-\frac{1}{2}\int_0^{t-t_0}e^{A\tau}BR^{-1}B^Te^{-A^T(t-\tau)}\boldsymbol{y}\,\mathrm{d}\tau \tag{23}$$

Using the boundary conditions $\boldsymbol{z}(t_0)$ and $\boldsymbol{z}(t_f)$, the constant vector $\boldsymbol{y}$ in Eq. (23) can be determined as

$$\boldsymbol{y}=-2\left(\int_0^{t_f-t_0}e^{A\tau}BR^{-1}B^Te^{-A^T(t_f-\tau)}\,\mathrm{d}\tau\right)^{-1}[\boldsymbol{z}(t_f)-e^{A(t_f-t_0)}\boldsymbol{z}(t_0)] \tag{24}$$

Hence, an explicit expression for the optimal balanced-energy controls is

$$\boldsymbol{u}(t)=R^{-1}B^Te^{-A^Tt}\left(\int_0^{t_f-t_0}e^{A\tau}BR^{-1}B^Te^{-A^T(t_f-\tau)}\,\mathrm{d}\tau\right)^{-1}\times(\boldsymbol{z}_f-e^{A(t_f-t_0)}\boldsymbol{z}_0) \tag{25}$$

IV. Three-Spacecraft Balanced-Energy Formation Reconfigurations

The problem of balanced-energy reconfigurations for a dual-spacecraft system was discussed in Sec. III. In this section, we explore the analogous three-spacecraft mission scenarios. Again adopting a double integrator model, the spacecraft governing translational dynamic equations will be as in Eq. (3). In this avenue, let $\boldsymbol{z}_1$ and $\boldsymbol{z}_2$ be, respectively, the vectors of relative states between the second and third spacecraft and the first spacecraft, i.e.,

$$\boldsymbol{z}_1(t):=x_1(t)-x_2(t)\quad\text{and}\quad\boldsymbol{z}_2(t):=x_1(t)-x_3(t)$$

The relative translational dynamics can then be written in the form of $\dot{\boldsymbol{z}}(t)=A\boldsymbol{z}(t)+B\boldsymbol{u}(t)$ because

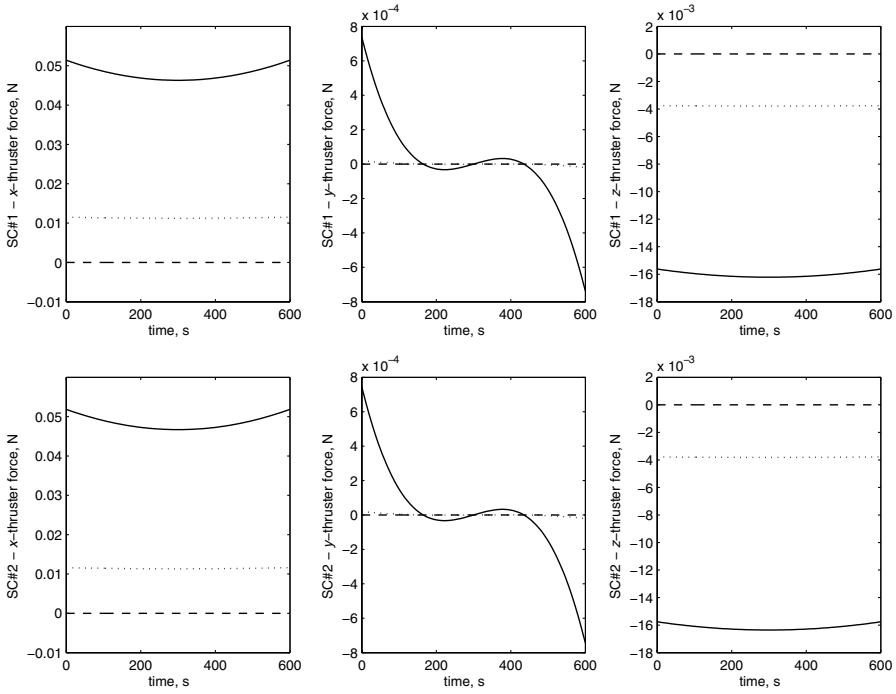

Fig. 7 Case 3: optimal control forces required for maintaining a given relative position.

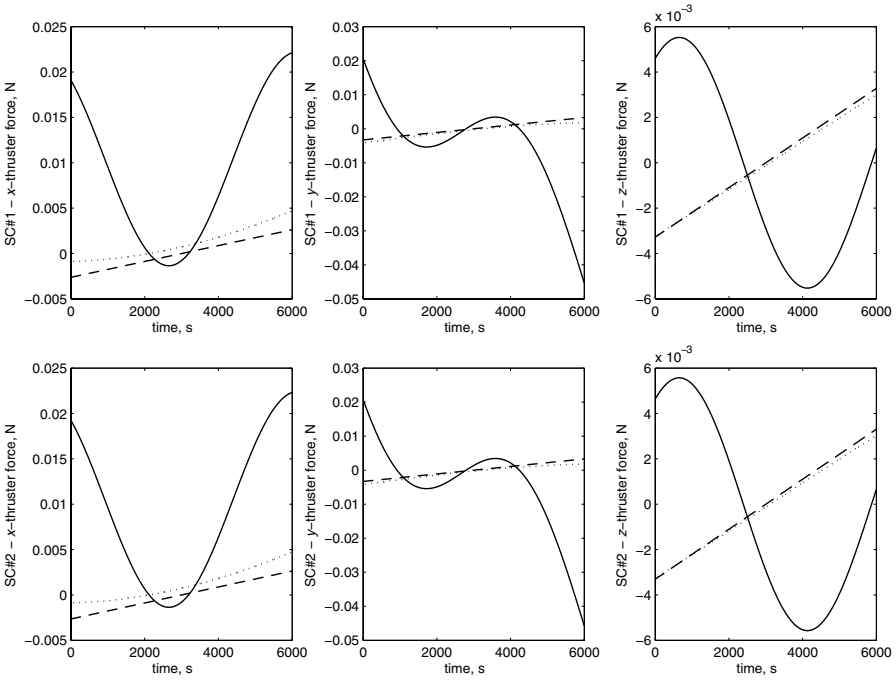

Fig. 8 Case 4: optimal control forces required for Case 2, with longer maneuver time.

$$\begin{bmatrix}\dot{z}_1(t)\\ \dot{z}_2(t)\end{bmatrix}=\begin{bmatrix}\hat{A} & 0\\ 0 & \hat{A}\end{bmatrix}\begin{bmatrix}z_1(t)\\ z_2(t)\end{bmatrix}+\begin{bmatrix}0 & 0 & 0\\ B_1 & -B_2 & 0\\ 0 & 0 & 0\\ B_1 & 0 & -B_3\end{bmatrix}\begin{bmatrix}\boldsymbol{u}_1(t)\\ \boldsymbol{u}_2(t)\\ \boldsymbol{u}_3(t)\end{bmatrix}$$

where

$$\hat{A}=\begin{bmatrix}0 & I\\ 0 & 0\end{bmatrix}\quad\text{and}\quad B_i=\frac{1}{m_i}I\quad\text{for } i=1,2,3$$

As the control objective for the formation is to consume optimal, yet balanced, energy on each spacecraft unit during the reconfiguration, we define the cost function $\mathcal{J}(u)$ as

$$\int_{t_0}^{t_f}\begin{bmatrix}\boldsymbol{u}_1(t)\\ \boldsymbol{u}_2(t)\\ \boldsymbol{u}_3(t)\end{bmatrix}^T R\begin{bmatrix}\boldsymbol{u}_1(t)\\ \boldsymbol{u}_2(t)\\ \boldsymbol{u}_3(t)\end{bmatrix}\mathrm{d}\tau=\int_{t_0}^{t_f}\boldsymbol{u}(t)^T R\boldsymbol{u}(t)\,\mathrm{d}\tau$$

with

$$R:=\begin{bmatrix}R_1+\hat{R} & -\hat{R} & 0\\ -\hat{R} & R_2+2\hat{R} & -\hat{R}\\ 0 & -\hat{R} & R_3+\hat{R}\end{bmatrix}$$

We note that the optimality conditions for the three-spacecraft scenario is now analogous to those in Sec. III.A. Nevertheless, the matrices A, B, and R and the vectors z and $\boldsymbol{u}$ are different from the dual-spacecraft case. First, solving for the costate $\lambda(t)$ from Eq. (7) leads to

$$\lambda(t) = e^{-A^T t}\boldsymbol{y}$$

again due to the special structure of the matrix A, the corresponding matrix exponential is $I - tA^T$. Next, to find the constant vector $\boldsymbol{y}$, we proceed to solve Eq. (10) subject to the boundary conditions on the relative state vector z. For this purpose, let

$$R^{-1} = \begin{bmatrix} \bar{R}_{11} & \bar{R}_{12} & \bar{R}_{13} \\ \bar{R}_{21} & \bar{R}_{22} & \bar{R}_{23} \\ \bar{R}_{31} & \bar{R}_{32} & \bar{R}_{33} \end{bmatrix}$$

then, from Eq. (10) one has

$$z(t) = \begin{bmatrix} I & (t-t_0)I & 0 & 0 \\ 0 & I & 0 & 0 \\ 0 & 0 & I & (t-t_0)I \\ 0 & 0 & 0 & I \end{bmatrix} z(t_0) + \frac{1}{2}[M(t) \odot^2 \tilde{R}]\boldsymbol{y} \tag{26}$$

where

$$M(t) = \begin{bmatrix} \frac{1}{6}(t-t_0)^2(t+2t_0) & -\frac{1}{2}(t-t_0)^2 \\ \frac{1}{2}(t-t_0)(t+t_0) & -(t-t_0) \end{bmatrix},$$

$$\tilde{R}_{11} = \left(\frac{1}{m_1^2}\bar{R}_{11} + \frac{1}{m_2^2}\bar{R}_{22} - \frac{1}{m_1 m_2}(\bar{R}_{21} + \bar{R}_{12})\right)I,$$

$$\tilde{R}_{12} = \left(\frac{1}{m_1^2}\bar{R}_{11} + \frac{1}{m_2 m_3}\bar{R}_{23} - \frac{1}{m_1 m_2}\bar{R}_{21} - \frac{1}{m_1 m_3}\bar{R}_{13}\right)I,$$

$$\tilde{R}_{21} = \left(\frac{1}{m_1^2}\bar{R}_{11} - \frac{1}{m_1 m_3}\bar{R}_{31} - \frac{1}{m_1 m_2}\bar{R}_{12} + \frac{1}{m_2 m_3}\bar{R}_{32}\right)I,$$

$$\tilde{R}_{22} = \left(\frac{1}{m_1^2}\bar{R}_{11} + \frac{1}{m_3^2}\bar{R}_{33} - \frac{1}{m_1 m_3}(\bar{R}_{31} + \bar{R}_{13})\right)I$$

and $\odot^2$ is the notation for a special block Kronecker product defined in the Appendix. Hence,

$$\boldsymbol{y} = 2H\left(z(t_f) - \begin{bmatrix} I & (t_f-t_0)I & 0 & 0 \\ 0 & I & 0 & 0 \\ 0 & 0 & I & (t_f-t_0)I \\ 0 & 0 & 0 & I \end{bmatrix} z(t_0)\right)$$

where

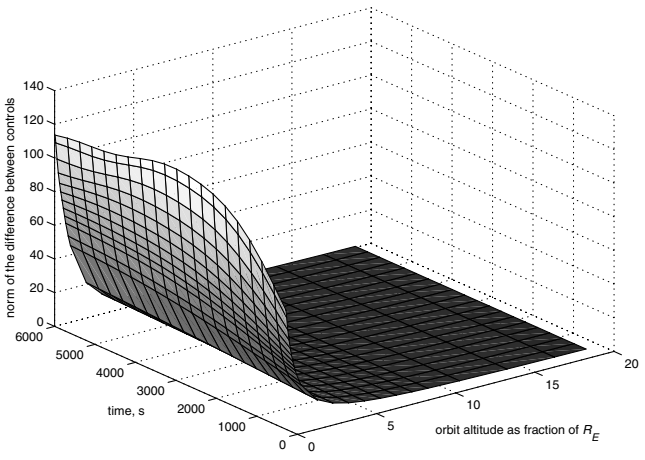

Fig. 9 The error $\mathcal{E}$ Eq. (28) as a function of orbit altitude and maneuver time.

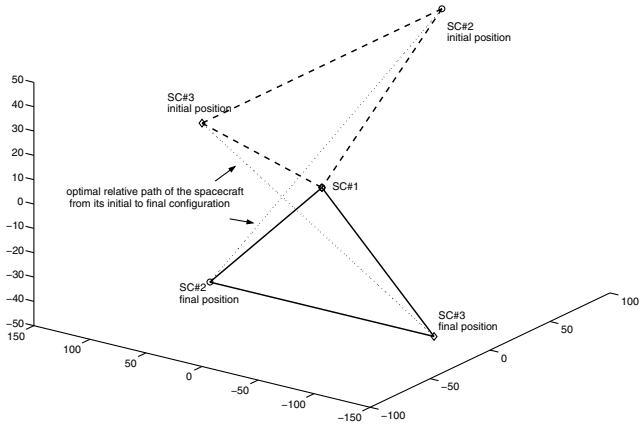

Fig. 10 A three-spacecraft balanced-energy reconfiguration maneuver.

$$H = M(t_f)^{-1} \odot^2 \tilde{R}^{-1} \tag{27}$$

and consequently, using Eq. (7), the optimal balanced-energy controls can explicitly be represented by

$$\boldsymbol{u}(t) = -R^{-1}B^T(I - tA^T)(M(t_f)^{-1} \odot^2 \tilde{R}^{-1}) \times \left(z(t_f) - \begin{bmatrix} I & (t_f-t_0)I & 0 & 0 \\ 0 & I & 0 & 0 \\ 0 & 0 & I & (t_f-t_0)I \\ 0 & 0 & 0 & I \end{bmatrix} z(t_0)\right)$$

V. Simulation Results

To validate the analytic results of Sec. III and IV, we carried out a set of numerical simulations that will be elaborated upon in this section. In the first set of simulations, two spacecraft with the same mass values ($m_1 = m_2 = 100$ kg) are commanded to change their relative positions from $z_0 = [20, 0, 0]^T$ to $z_f = [100, 100, 100]^T$ m in 10 min. The weighting matrices R_1 and R_2 are set to the identity matrix I, and $\hat{R} = \beta I$, with $\beta = 350$ for all cases. Figure 4 depicts the control forces in the x–y–z-frame for each spacecraft: the dashed lines are the controls corresponding to the deep-space motion, whereas the dotted lines pertain to the motion in an orbit with an altitude equal to Earth's radius; the solid lines are the control forces for a reference orbit of 1500 km above Earth's surface. As expected, control forces are equal but in opposite directions. The total fuel expenditure for carrying out the required reconfigurations in deep space, $h = R_E$, and $h = 1500$ km are, respectively, 17.8571, 17.8630, and 17.9645 g for each spacecraft.[‖] The second case is similar to the first with the exception that the spacecraft pair has distinct mass values of $m_1 = 200$ and $m_2 = 100$ kg. Figure 5 depicts the corresponding time history for the spacecraft control forces. The forces are equal but not in opposite directions (as they are in the previous case). The total amount of fuel required to carry out this maneuver in deep space (dashed), for $h = R_E$ (dotted), and for $h = 1500$ km (solid) are, respectively, 70.2214, 70.2441, and 70.6439 g, for the first spacecraft, and 70.825, 70.8480, and 71.2513 g for the second spacecraft. Figure 6 shows the relative distance between the spacecraft in the formation near a reference orbit of $h = 1500$ km. The dashed line is the time history for the dual-spacecraft relative distance when the computed control force is fed into differential equations suitable for the deep-space setting (i.e., double integrator dynamics), and the solid line is when the deep-space controls are fed to the Hill's dynamics suitable for near-Earth

[‖]The fuel is computed via $[1000/(\mathrm{g\,Isp})]\int_{t_0}^{t_f} \| \boldsymbol{u}(t) \| \, dt$ with Isp set to 400 s.

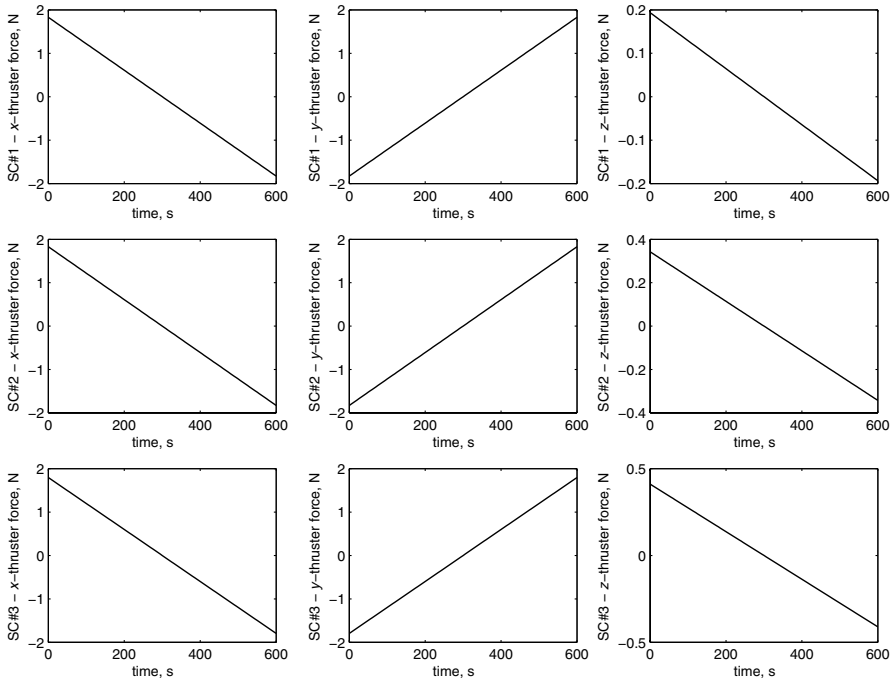

Fig. 11 The deep-space optimal controls time history for the balanced-energy three-spacecraft reconfiguration.

maneuvers. These figures clearly show that for near-Earth formations, the calculated deep-space controls do not possess the required optimality properties.

Case 3 is a follow up to the scenario discussed earlier: the pair of spacecraft for case 2 are now commanded to maintain their relative position at $z_0 = z_f = [100, 100, 100]^T$ m. Evidently, no control forces are required to maintain the previous configuration in deep space when the initial relative velocity is zero. However, in a near-Earth orbit, control forces are constantly needed to maintain the desired relative position; Fig. 7 shows the spacecraft control forces for this scenario. The total fuel expenditure needed to maintain the aforementioned relative position for deep space (dashed), $h = R_E$ (dotted), and $h = 1500$ km (solid) are, respectively, 0, 2.3109, and 9.824 g for each spacecraft. Table 1 summarizes the preceding three case studies.

To further examine the effect of time and reference orbit altitude on the optimality properties of the control forces, in the fourth set of simulation studies two spacecraft with mass values of 200 and 100 kg are commanded to change their relative position from $[20, 0, 0]^T$ to $[100, 100, 100]^T$ m in 100 min. In Fig. 8, the dotted lines depict the control forces to accomplish this maneuver in a $4R_E$ altitude orbit. This is indeed very similar to the deep-space controls (dashed line), whereas the control forces for the same maneuver in a 1500 km altitude orbit (solid line) is drastically different.

In view of these observations, we conclude that for short duration formation reconfigurations in high altitude orbits, the deep-space dynamics can effectively be employed for a formation's optimal control and maneuver design. To further quantify this assertion, we carried out an extensive set of simulations. In this avenue, two spacecraft units with mass values of 200 and 100 kg, respectively, are commanded to reconfigure from $[100, 100, 100]^T$ to $[20, 0, 0]^T$ m relative position, within a wide range of maneuver times and distinct reference orbits. The control error norms are then computed as the integral of the norm of the difference between optimal controls computed for each case via the Hill's dynamics and the corresponding deep-space optimal control forces, i.e.,

$$\mathcal{E}\,(t_f - t_0,\ \text{altitude}) = \int_{t_0}^{t_f} \| \boldsymbol{u}(t) - \boldsymbol{u}_{\text{deepspace}}(t) \|_2 \, \mathrm{d}t \qquad (28)$$

where $\boldsymbol{u}(t)$ is the optimal control computed for the formation via the Hill's dynamics at a given altitude [see Eq. (25)]. As depicted in Fig. 9, there is an exponential dependence of this error on the inverse of the orbit altitude. Furthermore, we note that this error is an increasing function of the maneuver time until it reaches the half period of the reference orbit, at which point it starts to decrease. For example, the 250 km reference orbit has a period of 89.51 min (for a quick comparison, a typical Space Shuttle flight altitude is 300 km), or a half period of 2676 s; this is exactly the point where the maximum error occurs.

Next, to investigate the fuel/energy optimality properties of balanced-energy optimal solutions, we carried out a set of simulations for deep-space dynamics, commanding the spacecraft to reconfigure from $z_0 = [20, 0, 0]^T$ to $z_f = [100, 100, 100]^T$ m in 20 min. The total fuel consumption for the scenario where $m_1 = m_2 = 150$ kg is 26.76 g, which is optimal both in the balanced sense and also with respect to the total fuel usage [see Sec. III.A and, in particular, our discussion following the inequality (19)].

For the three-spacecraft reconfiguration scenarios, mass values of $m_1 = 110$, $m_2 = 100$, and $m_3 = 120$ kg, are chosen for our simulations. The objective is to reconfigure the formation from the initial relative position vector $[100, 0, 50, -100, 0, 50]^T$ m to the final relative position vector $[0, 100, -50, 0, -100, -50]^T$ m. According to our convention in Sec. IV, the first three elements in each relative state vector represent the position of the second spacecraft relative to the first. Analogously, the second three element

Table 1 Comparison of spacecraft (sc) fuel usage in different scenarios

				Mass, kg		Fuel consumption, g		
Case	z_0, m	z_f, m	t_f, s	sc #1	sc #2	$h = 1500$	$h = R_E$	Deep space
1	$[20, 0, 0]^T$	$[100, 100, 100]^T$	600	100	100	17.965	17.863	17.857
2	$[20, 0, 0]^T$	$[100, 100, 100]^T$	600	200	100	70.644	70.244	70.221
3	$[100, 100, 100]^T$	$[100, 100, 100]^T$	600	200	100	9.824	2.311	0.000

set represents the relative position of the third and the first spacecraft. The weighting matrices R_1, R_2, and R_3 are all chosen to be the identity matrix, and $\hat{R} = \beta I$, where β is chosen to minimize the ratio of the imbalance in spacecraft energy usage and the total spacecraft consumed energy (in our case $\beta = 679$). Figure 10 depicts the corresponding initial and final formation configurations. In this figure, the relative state trajectory for each spacecraft is shown with respect to the noninertial frame attached to the first spacecraft. We note that none of the spacecraft move in a straight-line trajectory inertially. The resulting optimal controls for the three-spacecraft formation are also shown in Fig. 11. The total energy for each spacecraft turns out to be 1155.00, 1200.00, and 1200.01 N · s, respectively.

VI. Conclusion

In this paper, the problem of balanced-energy reconfiguration for two- and three-spacecraft formations has been considered using optimal control techniques. In this direction, an analytical solution for the relative reconfiguration of two- and three- spacecraft was derived and simulated for various mission scenarios. In particular, it was shown that the validity of a double integrator model for studying multiple spacecraft reconfiguration problems in Earth's gravitational field critically depends on the formation maneuver time and its operational altitude. To further expand on this assertion, the corresponding optimal control forces were computed for formations near a circular reference orbit via the Hill's equations. These forces were then compared with those derived using the double integrator model, often employed for deep-space maneuver design. Numerical simulations were then carried out for different mission scenarios to demonstrate the effect of orbit altitude, maneuver time, spacecraft mass values, and objective functional weighting matrices, on the control forces and their optimality properties.

Appendix: Block Kronecker Product

In this paper, a special block Kronecker product $\odot^k$ between matrices M and R has been defined to further compact the derived equations. This matrix operation first partitions R into k^2 submatrices and then takes the Kronecker product of M with each partition of R, i.e.,

$$M \odot^k R = \begin{bmatrix} M \otimes R_{11} & \cdots & M \otimes R_{1k} \\ \vdots & \ddots & \vdots \\ M \otimes R_{k1} & \cdots & M \otimes R_{kk} \end{bmatrix}$$

Using the properties of the Kronecker product it can then be shown that

$$(M \odot^k R)(M^{-1} \odot^k R^{-1}) = I$$

or equivalently,

$$(M \odot^k R)^{-1} = M^{-1} \odot^k R^{-1}$$

where $\odot^k$ partitions R^{-1} the same way that it partitions R.

Acknowledgments

The research of the first two authors was supported by National Science Foundation under grant CMS-0301753 and a grant from Jet Propulsion Laboratory, California Institute of Technology, under a contract with the National Aeronautics and Space Administration. The research of F. Y. Hadaegh was carried out at Jet Propulsion Laboratory, California Institute of Technology, under a contract with the National Aeronautics and Space Administration. The authors would also like to gratefully thank the Associate Editor and the anonymous reviewers for their very helpful comments and suggestions.

References

[1] *Terrestrial Planet Finder: Origins of Stars, Planets, and Life*, edited by C. A. Beichman, N. J. Woolf, and C. A. Lindensmith, Jet Propulsion Laboratory Paper 99-003, California Inst. of Technology, May 1999.

[2] DARWIN Space Infrared Interferometer Project [Online]: http://en.wikipedia.org/wiki/Darwin_(ESA).

[3] Gorham, P. W., Folkner, W. M., and Blackwood, G. B., Enabling Concepts for a Dual Spacecraft Formation: Flying Optical Interferometer for NASA's ST3 Mission, *Working on the Fringe*, Vol. 194, Publications of the Astronomical Society of the Pacific Conference Series, 1999, pp. 395–400.

[4] Beard, R., Lawton, J., and Hadaegh, F. Y., "A Coordination Architecture for Spacecraft Formation Control," *IEEE Transactions on Control Systems Technology*, Vol. 9, No. 6, Nov. 2001, pp. 777–790.

[5] Kang, W., Sparks, A., and Banda, S., "Coordinated Control Of Multisatellite Systems," *Journal of Guidance, Control, and Dynamics*, Vol. 24, No. 2, 2001, pp. 360–368.

[6] Tillerson, M., Inalhan, G., and How, J. P., "Coordination and Control of Distributed Spacecraft Systems Using Convex Optimization Techniques," *International Journal of Robust and Nonlinear Control*, Vol. 12, Nos. 2–3, 2002, pp. 207–242.

[7] Schetter, T., Campbell, M. E., and Surka, D., "Multiple Agent-Based Autonomy for Satellite Constellations," , *Journal of Artificial Intelligence Research*, Vol. 145, Nos. 1–2, April 2003, pp. 147–180.

[8] Smith, R. S., and Hadaegh, F. Y., "Control of Deep Space Formation-Flying Spacecraft; Relative Sensing and Switched Information," *Journal of Guidance, Control, and Dynamics*, Vol. 28, No. 1, 2005, pp. 106–114.

[9] Kim, Y., Mesbahi, M., and Hadaegh, F. Y., "Dual-Spacecraft Formation Flying: Optimal Collision-Free Reconfigurations," *Journal of Guidance, Control, and Dynamics*, Vol. 26, No. 2, 2003, pp. 375–379.

[10] Hussein, I. I., "Motion Planning for Multi-Spacecraft Interferometric Imaging Systems," Ph.D. Dissertation, University of Michigan, Ann Arbor, MI, 2005.

[11] Wang, P. K. C., and Hadaegh, F. Y., "Coordination and Control of Multiple Microspacecraft Moving in Formation," *Journal of the Astronautical Sciences*, Vol. 44, No. 3, 1996, pp. 315–355.

[12] Mesbahi, M., and Hadaegh, F. Y., "Formation Flying Control of Multiple Spacecraft via Graphs, Matrix Inequalities, and Switching," *Journal of Guidance, Control, and Dynamics*, Vol. 24, No. 2, 2001, pp. 369–377.

[13] Robertson, A., Inalhan, G., and How, J. P., "Spacecraft Formation Flying Control Design for the Orion Mission," *Proceedings of AIAA Guidance, Navigation, and Control Conference*, AIAA Paper 1999-4266, 1999.

[14] Tillerson, M., Breger, L., and How, J. P., "Distributed Coordination and Control of Formation Flying Spacecraft," *Proceedings of the American Control Conference*, June 2003, pp. 1740–1745.

[15] Vadali, S. R., Vaddi, S. S., and Alfriend, K. T., "An Intelligent Control Concept for Formation Flying Satellites," *International Journal of Robust and Nonlinear Control*, Vol. 12, Nos. 2–3, 2002, pp. 97–115.

[16] Davis, J., "Measuring Stars with High Angular Resolution: Current Status and Future Prospects," *Calibration of Fundamental Stellar Quantities*, edited by D. S. Hayes, L. E. Pasinetti, and A. G. D. Philips, Reidel, Dordrecht, The Netherlands, 1985.

[17] Born, M., and Wolf, E., *Principles of Optics*, 6th ed., Cambridge Univ., Cambridge, U.K., 1997.

[18] Stachnik, R., Ashlin, K., and Hamilton, K., Space-Station-SAMSI: A Spacecraft Array for Michelson Spatial Interferometry, *Bulletin of the American Astronomical Society*, 16, 1984, 818–827.

[19] Kong, E. M., Spacecraft Formation Flight: Exploiting Potential Fields, Ph.D. Dissertation, Massachusetts Inst. of Technology, Cambridge, MA, 2002.

[20] Mesbahi, M., and Hadaegh, F. Y., "Mode and Logic-Based Switching for the Formation Flying Control of Multiple Spacecraft," *Journal of the Astronautical Sciences*, Vol. 49, No. 3, 2001, pp. 443–468.

[21] Bailey, C. A., McLain, T. W., and Beard, R. W., "Fuel Saving Strategies for Dual Spacecraft Interferometry Missions," *Journal of the Astronautical Sciences*, Vol. 49, No. 3, 2001, pp. 469–488.

[22] Papadimitriou, C. H., and Steiglitz, K., *Combinatorial Optimization: Algorithms and Complexity*, Dover, New York, 1998.

[23] Boccaletti, D., and Pucacco, G., *Theory of Orbits 1: Integrable Systems and Non-Perturbative Methods*, Springer, New York, 2001.

[24] Sidi, M., *Spacecraft Dynamics and Control*, Cambridge Univ., Cambridge, U.K., 1997.